ISSN 1070-4272, Russian Journal of Applied Chemistry, 2019, Vol. 92, No. 1, pp. 1−8. © Pleiades Publishing, Ltd., 2019.
Russian Text © M.Zh. Burkeev, T.O. Khamitova, D. Havliček, A.Zh. Sarsenbekova, S.Zh. Davrenbekov, E.M. Tazhbaeva, G.E. Kozhabekova, Zh.K. Imanbekova, A.N. Bolatbai, 2019, published in Zhurnal Prikladnoi Khimii, 2019, Vol. 92, No. 1, pp. 5−12.

MACROMOLECULAR COMPOUNDS AND POLYMERIC MATERIALS

Synthesis, Characterization, and Catalytic Properties of Metal–Polymer Complexes Based on Copolymers of Polyethylene(propylene) Glycol Maleates with Acrylic Acid

M. Zh. Burkeev[a], T. O. Khamitova[a,*], D. Havliček[b], A. Zh. Sarsenbekova[a], S. Zh. Davrenbekov[a], E. M. Tazhbaev[a], G. E. Kozhabekova[a], Zh. K. Imanbekova[a], and A. N. Bolatbai[a]

[a] *Buketov State University, Karaganda, 100028 Kazakhstan*
[b] *Charles University, Prague, Czech Republic*
**e-mail: khamitova.t@inbox.ru*

Received July 2, 2018; Revised October 1, 2018; Accepted October 10, 2018

Abstract—New mono- and bimetallic polymer nanocomposites based on polyethylene(propylene) glycol maleates with acrylic acid and silver and nickel metals were prepared and studied. Metal particles were immobilized into copolymer supports by reduction of Ag^+ and Ni^{2+} ions from solution of their nitrates to Ag^0 and Ni^0 in the presence of a catalyst, a solution of silver chloride in aqueous ammonia. The structure and composition of the complexes were determined by spectroscopy, calorimetry, microscopy, and chromatography. The catalytic activity was studied using pyridine hydrogenation as a model reaction.

Keywords: polyethylene glycol maleate, polypropylene glycol maleate, catalysis, nanoparticles, metal–polymer complex, hydrogenation

DOI: 10.1134/S1070427219010014

Numerous papers deal with the synthesis and properties of nanoparticles and nanosystems [1, 2]. Various procedures for synthesis of nanoparticles are analyzed in detail in [3–5], and properties of nanoparticles, in [6–8].

Increased researchers' interest in polymer-stabilized metal nanoparticles is caused by the possibility of controlling the growth kinetics, size, and stability of nanoparticles, which ultimately determines their catalytic, magnetic, electrical, optical, medicobiological, and other properties. A decrease in the catalyst particle size to the nanometer level allows the area of contact of the polymer with the reaction medium to be increased and thus the catalysis efficiency to be considerably enhanced; the gel matrix prevents coagulation and oxidation of the particles. Therefore, synthesis of new metal–polymer matrix nanocatalysts opens wide prospects for using them in catalysis, petroleum industry, organic synthesis, etc., and search for new catalytic systems, including nanocatalysts, exhibiting high activity and selectivity is a topical problem.

Metal–polymer complexes (MPCs) based on polyethylene glycol maleate–acrylic acid (*p*-EGM : AA) and polypropylene glycol maleate–acrylic acid (*p*-PGM : AA) copolymers with transition metals (Ni, Co) were synthesized previously [9]. The studies demonstrated the possibility of using copolymers of poly(ethylene)propylene glycol maleates with acrylic acid as a matrix for preparing effective metal–polymer complexes for hydrogenation of organic compounds. The mean diameter of nanoparticles, 112 nm, was determined by electron microscopy and dynamic light scattering. The particles have spherical shape and are uniformly distributed over the polymer cross section. The content of nickel and cobalt in the complexes is

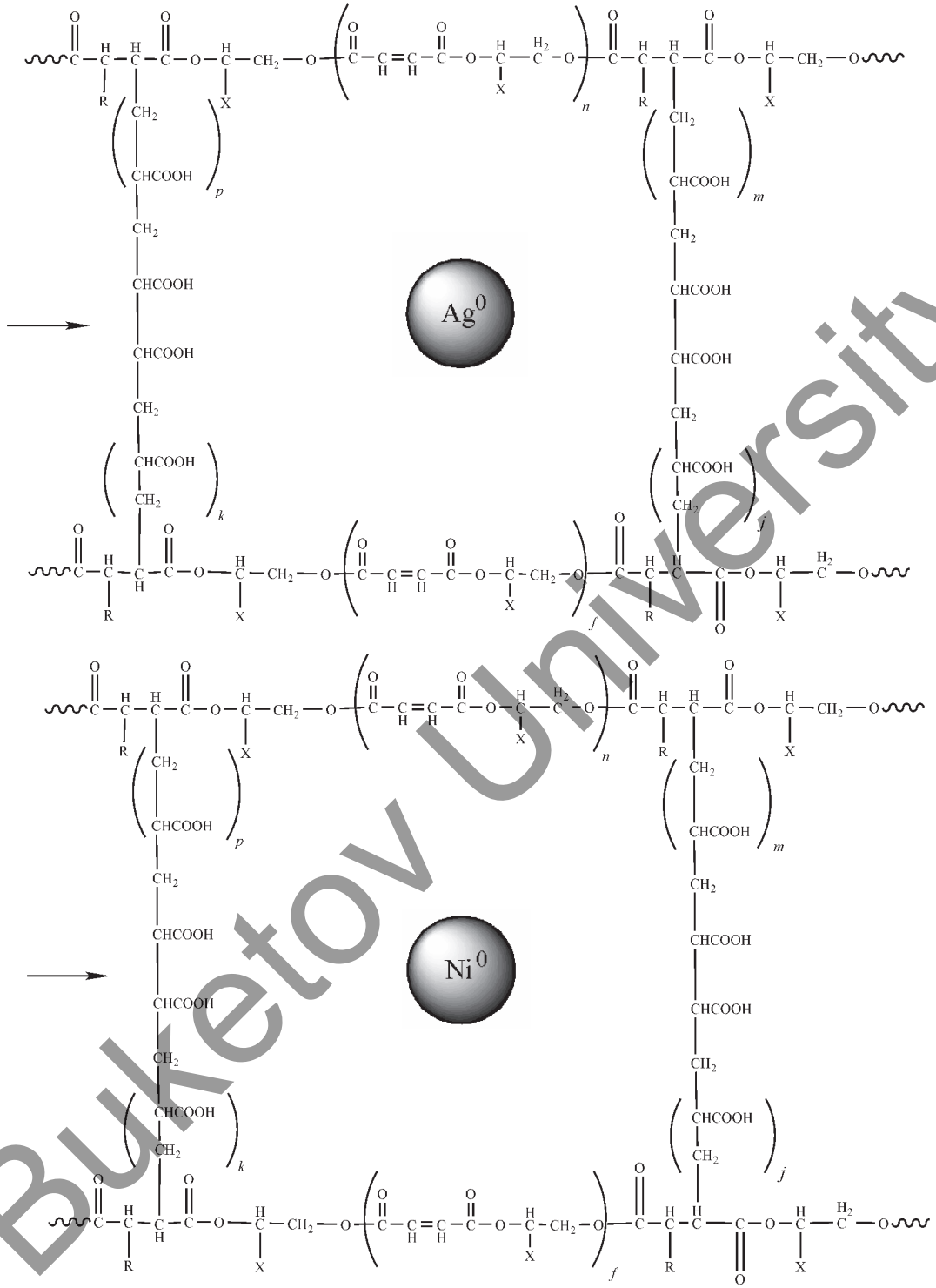

Fig. 1. Structural fragments of monometallic polymer complexes. X = H, CH_3; R is initiator radical.

0.52 and 0.48 wt % in *p*-EGM : AA copolymer and 0.49 and 0.51 wt % in *p*-PGM : AA copolymer, respectively. The temperature elevation from 25 to 40°C allows the pyridine hydrogenation rate to be appreciably increased owing to the catalyst activation and increase in the number of active sites of the catalyst as a result of swelling of the polymer network and its transition from the contracted globular state to the unrolled state.

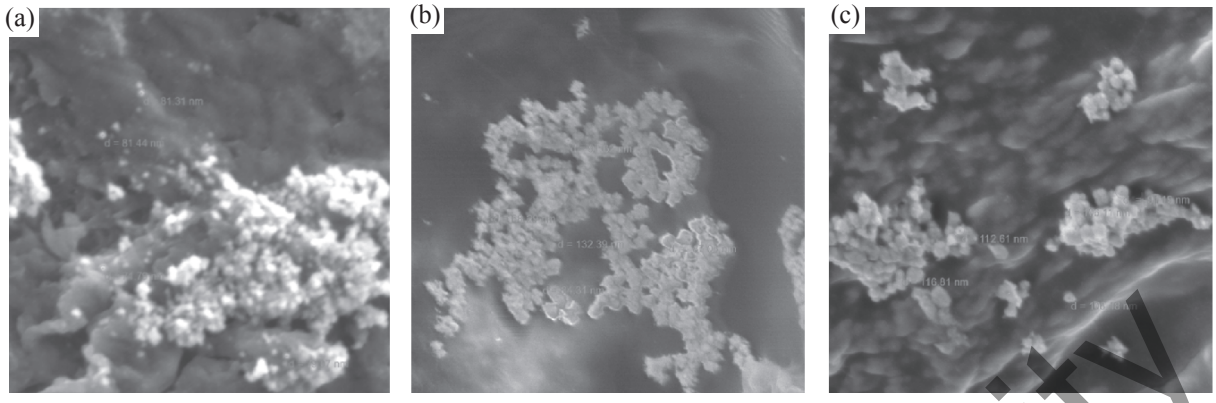

Fig. 2. Electron-microscopic images of (a) *p*-PGM : AA/Ni, (b) *p*-PGM : AA/Ag, and (c) *p*-PGM : AA/Ag–Ni.

This study was aimed at synthesis and characterization of new catalytically active mono- and bimetallic nanocomposites based on a smart polymer matrix, *p*-EGM (*p*-PGM) : AA, with noble and transition metals. Such data will expand the theoretical concepts of the formation of metal–polymer complexes and will contribute to the theory and practice of nanocomposite preparation.

EXPERIMENTAL

Synthesis of *p*-EGM : AA/Ag, *p*-EGM : AA/Ni, *p*-EGM : AA/Ag–Ni, *p*-PGM : AA/Ag, *p*-PGM : AA/Ni, and *p*-PGM : AA/Ag–Ni. Metal particles were immobilized into supports of 14.8/85.2 wt % *p*-EGM : AA copolymers and of 15.1/84.9 wt % *p*-PGM : AA copolymers by reduction of Ni^{2+} and Ag^{+} from a 0.1 M solution of their nitrates to Ni^{0} and Ag^{0} with sodium hypophosphite in the presence of a catalyst, solution of silver chloride in aqueous ammonia. The reduction of Ni^{2+} and Ag^{+} in the bulk of the *p*-EGM : AA or *p*-PGM : AA polymer matrix occurs in several steps: incorporation of Ni^{2+} and Ag^{+} ions into the polymer matrix; diffusion of the reagents in the polymer matrix; reaction of nickel and silver nitrates with sodium hypophosphite to form metal nanoparticles (NPs).

The first group includes metal–polymer complexes of cross-linked *p*-EGM : AA copolymer with nickel and silver: *p*-EGM : AA/Ag (MPC-1), *p*-EGM : AA/Ni (MPC-2), and *p*-EGM : AA/Ag–Ni (BPC-1), and the second group, metal-polymer complexes *p*-PGM : AA/Ag (MPC-3), *p*-PGM : AA/Ni (MPC-4), and *p*-PGM : AA/Ag–Ni (BPC-2). The main structural fragments of MPC-1 and MPC-3 are shown in Figs. 1a and 1b, respectively.

The structure, morphology, and elemental composition of the complexes were studied by scanning electron microscopy with a MIRA 3TESCAN device (Oxford Instruments, 2012) equipped with an X-Act high-performance silicon drift detector for elemental analysis at an accelerating voltage of 20 kV (Fig. 2). Transmission electron microscopic (TEM) images of ultrathin samples were taken with a JEOL JEM-2100 200-keV universal thermal field device (Japan) on the base of the Chair of Analytical and Inorganic Chemistry, Charles University, Prague, Czech Republic. The resolution at the optimum working distance was 0.8 nm at 1 kV. The heat resistance of the composites was evaluated by thermal gravimetric analysis with a LabSYSEvo (2014) synchronous TGA/DTA/DSC analyzer in the temperature interval 30–1000°C in an alumina crucible at a heating rate of 5 deg min^{-1} in air at a flow rate of 30 mL min^{-1} and a sample weight of 20 mg (Fig. 3). The amount of the adsorbed metal in the complex was determined with a Laesmatrix (2012) laser emission spectrometer equipped with a two-pulse YAG : Nd (neodymium-doped yttrium aluminum garnet) laser with the generated radiation wavelength of 1064 nm, radiation pulse energy of 100 mJ, pulse length of 10–15 ns, and pulse repetition frequency of 1–20 Hz by processing the spectra with the appropriate software and calculating the weight fractions of the elements from the intensities of their characteristic spectrum lines (Fig. 4).

Pyridine hydrogenation was performed in a temperature-controlled electrocatalytic cell with a diaphragm. The anode and cathode compartments were separated with an MK-40 membrane diaphragm in accordance with [10]. Platinum grid served as an anode, and a copper plate (conductor of first kind) with a surface area

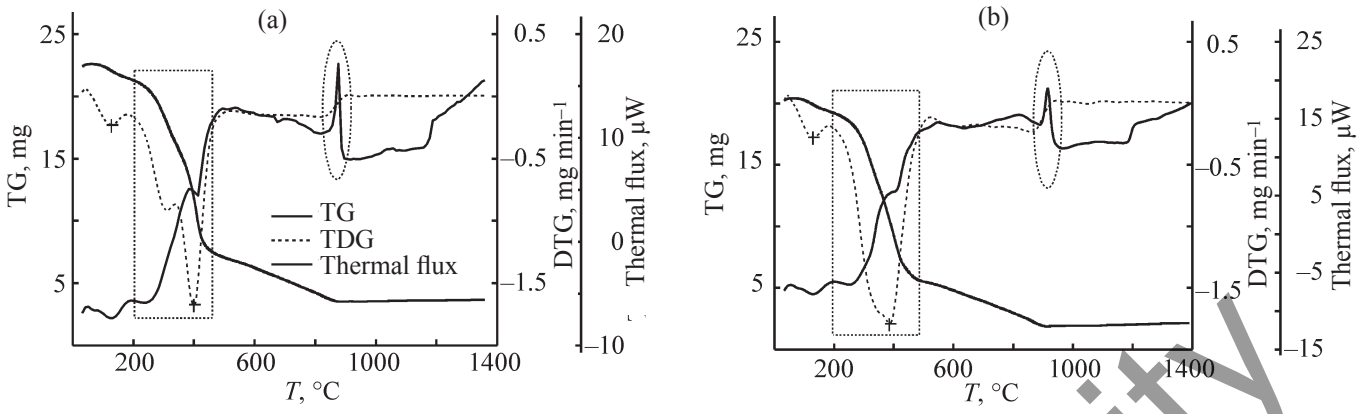

Fig. 3. Thermograms of the (a) *p*-EGM : AA polymer matrix and (b) *p*-EGM : AA/Ag^0 metal–polymer complex.

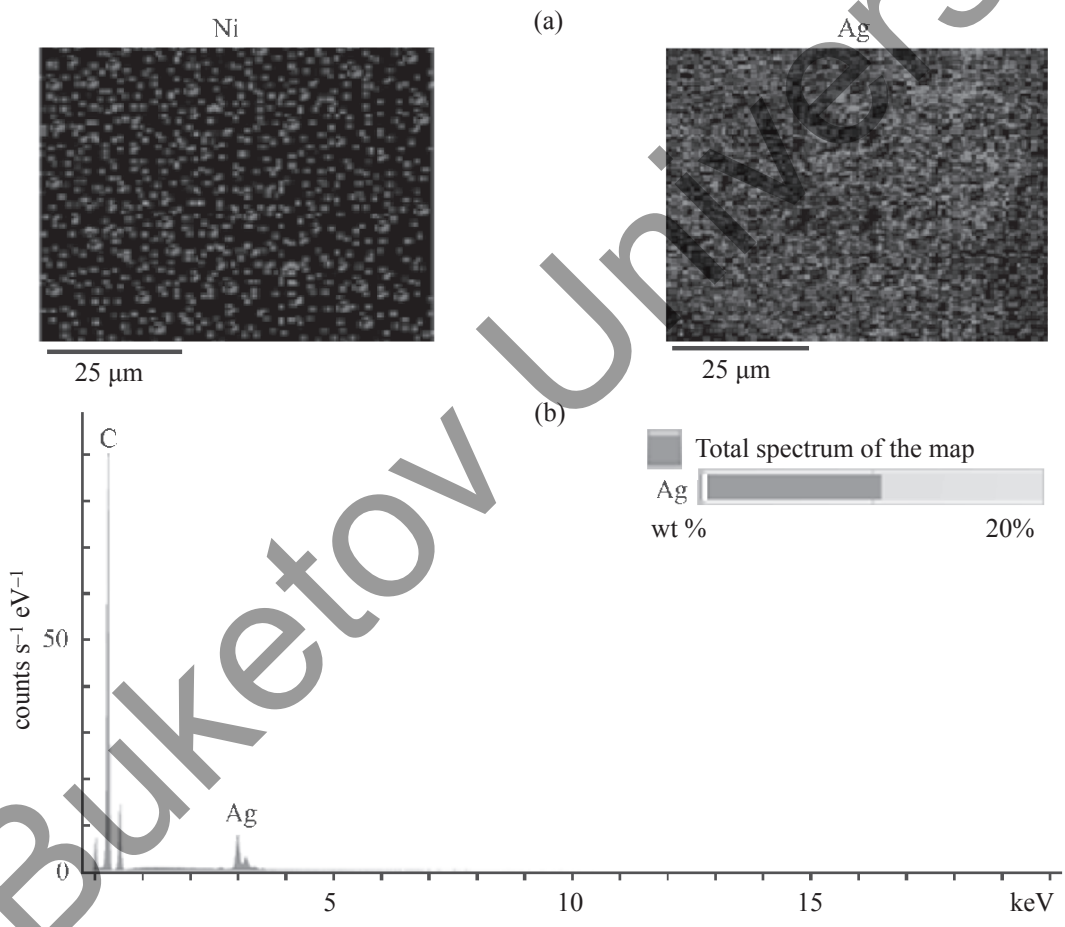

Fig. 4. (a) Micrographs of the Ni and Ag distribution on the surface of the *p*-EGM : AA matrix and (b) spectrum of the composite.

of 0.048 dm^2, tightly fitting to the electrolyzer bottom and acting as the catalyst support, as a cathode. Pyridine hydrogenation was performed at different currents and temperatures. The process consisted of the following steps: (1) start of the process: introduction of solutions and control of process conditions; a 20% NaOH solution was used as an anolyte, and a 5% NaOH solution, as a catholyte; (2) saturation: the metal–polymer complexes obtained were saturated for 30 min with electrocatalytic hydrogen in the cathode compartment until the volume

ratio of the released H_2 and O_2 in the burettes became equal to 2 : 1; (3) hydrogenation: a weighed portion of the substrate (pyridine) was introduced into the cathode compartment, and the volumes of the released hydrogen and oxygen were recorded at 2-min intervals; the hydrogenation was performed until the hydrogen uptake fully ceased. The pyridine reduction rate W_{H_2} (mol s^{-1}) and hydrogen utilization coefficient were determined from the amount of hydrogen taken up.

The hydrogenation products were analyzed with an Agilent 7890A chromatograph equipped with a 5975C mass-selective detector. The catholyte was extracted with diethyl ether in 1 : 1 ratio. The samples were pretreated with a CryoMill vibration mill (Retsch, Germany, 2015).

RESULTS AND DISCUSSION

One of specific features of metal–polymer composites is that active components in the form of nano- and microcrystals are distributed in the bulk of the polymer matrix, which stabilizes them, preserving the high activity of metal particles and remaining a highly elastic support. The metal/polymer composites combining unique properties of the polymer and metals acquire some new properties that the materials taken separately do not have. These materials of a new class are used as electrode materials for making high-sensitivity selective electrodes, chemical sensors, and various detectors giving response to ions and molecules of dissolved substances being analyzed in monitoring of various natural objects. Metal/polymer composites are efficient as catalysts and electrocatalysts [11]. Nanoparticles in the polymer matrix ensure increased performance due to higher specific surface area compared to common catalysts based on dispersed metals.

Nanocomposite materials incorporating dispersed particles of noble (Ag, Au, Pt, Pd) and base transition (Cu, Ni, Fe, Co) metals [12] are of particular interest because of the possibility of using them in new electric, magnetic, catalytic, and sensor devices. Combination of individual properties of the metal and polymer gives positive effects, including enhancement of the catalytic activity.

The structure of all the mono- and bimetallic polymer complexes synthesized was confirmed by IR spectroscopy (cm^{-1}):

– *p*-EGM : AA/Ag, dark dray powder: 3429 (O–H); 2928 (C–H_{st}); 2854, 2357 (C–H_{st}, CH_2–N_{st}); 1639 [C=O_{bound} with OH(COOH)]; 1462 (CH_2 δ); 1165, 1095 (CH_3 δ); 552 (Me);

– *p*-EGM : AA/Ni, light green powder: 3433 (O–H); 2932 (C–H_{st}); 2847, 2357 (C–H_{st}, CH_2–N_{st}); 1619 [C=O_{bound} with OH(COOH)]; 1458 (CH_2 δ); 1169, 1114 (CH_3 δ); 543 (Me);

– *p*-EGM : AA/Ag–Ni, gray powder: 3410 (O–H); 2960 (C–H_{st}); 2831 (C–H_{st}, CH_2–N_{st}); 1623 [C=O_{bound} with OH(COOH)]; 1172 (CH_3 δ); 603 (Me);

– *p*-PGM : AA/Ag, dark gray powder: 3420 (O–H); 2930 (C–H_{st}); 2844, 2377 (C–H_{st}, CH_2–N_{st}); 1649 [C=O_{bound} with OH(COOH)]; 1480 (CH_2 δ); 1171 (CH_3 δ); 503 (Me);

– *p*-PGM : AA/Ni, light green powder: 3441 (O–H); 2978 (C–H_{st}); 2360 (C–H_{st}, CH_2–N_{st}); 1716 [C=O_{bound} with OH(COOH)]; 1454 (CH_2 δ); 1165 (CH_3 δ); 509 (Me);

– *p*-PGM : AA/Ag–Ni, gray powder: 3410 (O–H); 2924 (C–H_{st}); 2843 (C–H_{st}, CH_2–N_{st}); 1628 [C=O_{bound} with OH(COOH)]; 1157 (CH_3 δ); 648 (Me).

The thermal behavior of the synthesized MPCs was studied for the *p*-EGM : AA/Ag^0 nanocomposite as example (Fig. 3b). In the thermal gravimetric analysis pattern of the *p*-EGM/AA : Ag^0 composite, the first endothermic peak at 30–100°C corresponds to the elimination of bound water, and the second peak, to the degradation of the *p*-EGM : AA copolymer at 200–900°C. At ~400°C, there is a strong exothermic effect caused by decomposition of the compound with the elimination of carboxy groups. This follows from a twofold decrease in the intensity of the bands at 1639 cm^{-1}. At ~855–900°C, the weight is stabilized. The total weight loss on heating to 900°C is 99.09%. Visually this transition is accompanied by blackening of the sample, apparently caused by the presence of Ag nanoparticles (~1%).

According to the MIRA 3 Tescan SEM data, the metal nanoparticle size depended on the pore size in the initial polymer matrices, *p*-EGM : AA and *p*-PGM : AA. For MPC-1,2 samples prepared from *p*-EGM : AA (14.8/85.2 wt %), the particle size was 80 ± 10 nm, which corresponds to the denser structure of the support. For MPC based on *p*-PGM : AA (15.1/84.9 wt %), the particle size was 85 ± 5 nm, in agreement with the TEM estimation of the pore size (Table 1). Figure 2 shows the electron micrographs of the MPCs of the second group: *p*-PGM : AA/Ag (MPC-3), *p*-PGM : AA/Ni, and *p*-PGM : AA/Ag–Ni.

Table 1. Main characteristics of the synthesized mono- and bimetallic polymer complexes

Complex	Matrix pore size, nm	Metal content of the composite, wt %, calculated/found	Particle size, nm	NP morphology	Mean number of nanoparticles per 25 μm
MPC-1	700 ± 150	10/9.02	71 ± 3	Sphere	1800 ± 150
MPC-2	700 ± 150	10/9.01	89 ± 5	Rhomb	1200 ± 100
MPC-3	800 ± 200	10/9.08	76 ± 5	Sphere	1700 ± 150
MPC-4	800 ± 200	10/9.10	93 ± 6	Rhomb	1230 ± 100
BPC-1	700 ± 150	10/9.16	98 ± 4	Sphere, rhomb	1550 ± 50 Ag and 300 ± 50 Ni
BPC-2	800 ± 200	10/9.00	104 ± 3	Sphere, rhomb	1600 ± 100 Ag and 350 ± 50 Ni

The EDX data show that the distribution of Ni^0 and Ag^0 over the polymer cross section is relatively uniform. The mean number of metal particles per 25 μm is ~1800 ± 100 for Ag and ~1200 ± 100 for Ni (Fig. 4). The Ag/Ni ratio is 60/40% in *p*-EGM : AA copolymer and 58/42% in *p*-PGM : AA copolymer (Table 1, Fig. 5).

The main characteristics of the synthesized mono- and bimetallic polymer complexes are given in Table 1.

The reaction rate in the presence of the mono- and bimetallic catalysts obtained was studied at I = 1–1.5 A and T = 30–35°C. The curve of the rate W of pyridine hydrogenation to piperidine vs. time t has three portions. The pyridine hydrogenation rate in the presence of BPC-1,2 increases gradually, reaches a maximum ~6–9 min after the start of the reaction, and then sharply decreases. In this period, according to the chromatographic data, the major product, piperidine, is accumulated in the reaction mixture in an amount from 30 to 40%. As seen from Table 2, the reaction rate in the presence of bimetallic systems increases by a factor of ~5–6 compared to monometallic nickel and by a factor of ~10–11 compared to the system without catalyst;

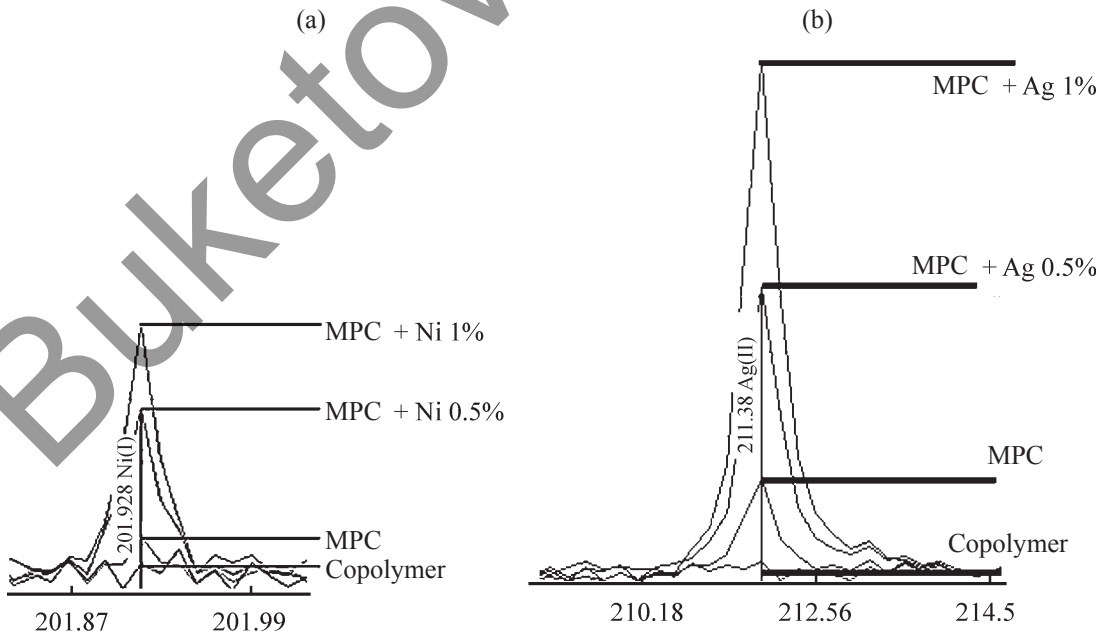

Fig. 5. Intensities of (a) Ni(I) (201.928) and (b) Ag(II) (211.38) peaks at varied metal weight.

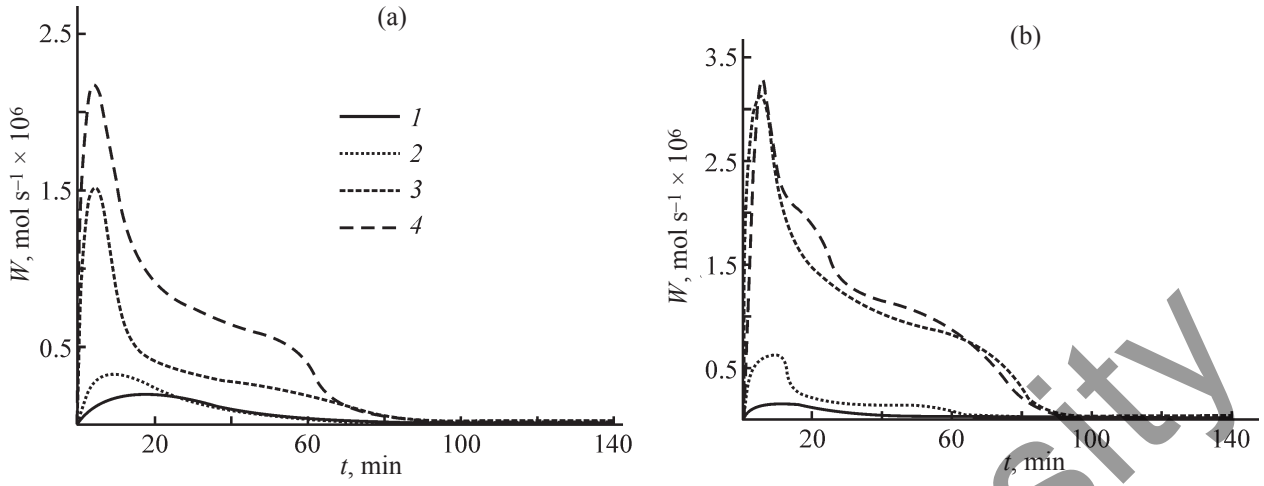

Fig. 6. Hydrogenation rate on different catalysts and without catalyst at a current of (a) 1 and (b) 1.5 A; T = 35°C. Catalyst: (*1*) none, (*2*) MPC-2, (*3*) MPC-3, and (*4*) BPC-1.

correspondingly, the selectivity to piperidine increases by a factor of ~3–4.

Our results show that the optimum conditions for electrocatalytic hydrogenation of pyridine are as follows: 1.5 A, 35°C, bimetallic catalyst *p*-EGM : AA/Ag–Ni (0.9% Me), on which the reaction rate and selectivity with respect to piperidine are the highest.

The results of experiments with repeated use of the bimetallic catalyst *p*-EGM : AA/Ag^0–Ni^0 (0.9%). are given in Table 3. As can be seen, the repeated use of the BPC-1 catalyst containing 0.9% Me leads to only a minor activity loss. It should be noted that the systems obtained can be readily separated from the reaction products and repeatedly used without activity loss.

Table 2. Conditions and results of pyridine hydrogenation on mono- and bimetallic catalysts and without them

Catalyst	T, °C	Current, A	Pressure, mmHg	Hydrogenation products, %			Reaction rate $W \times 10^6$, mol s^{-1}
				pyridine	piperidine,	secondary products	
None	30	1	762	91.8	8.2	–	0.1
		1.5	764	90.1	9.9	–	0.2
	35	1	751	90.6	9.4	–	0.2
		1.5	755	88.8	11.2	–	0.2
MPC-2	30	1	758	80.9	19.1	–	0.3
		1.5	758	77.7	22.3	1.2	0.5
	35	1	763	79.3	20.7	1.1	0.3
		1.5	760	75.8	24.3	1.5	0.6
BPC-1	30	1	776	11	84.82	4.2	1.8
		1.5	767	9.3	86.78	3.9	3.1
	35	1	768	5.6	87.32	5.1	2.2
		1.5	767	5.8	89.7	4.5	3.3
MPC-1	30	1	775	25.5	68.26	6.2	1.7
		1.5	771	20.7	74.82	4.5	2.4
	35	1	752	15.5	79.11	5.4	1.5
		1.5	752	12.8	79.15	8.1	3.1

Table 3. Results of repeated use of the bimetallic catalyst *p*-EGM : AA/Ag^0–Ni^0 (0.9% Ag–Ni). Conditions: T = 35°C, current 1.5 A

Repeated use	Reaction rate $W \times 10^6$, mol s^{-1}	Target product yield, %
After 7 days	3.2	88.8
After 14 days	3.1	81.5
After 20 days	3.0	75.3
After 1 month	2.8	68.7

CONCLUSIONS

New mono- and bimetallic polymer complexes *p*-EGM : AA/Ag, *p*-EGM : AAK/Ni, *p*-EGM : AA/Ag–Ni, *p*-PGM : AA/Ag, *p*-PGM : AA/Ni, and *p*-PGM : AA/Ag–Ni, exhibiting catalytic activity in hydrogenation, were prepared by immobilization of metal particles in supports of *p*-EGM(PGM) : AA copolymers. The reaction can be performed under mild conditions with high yield using the *p*-EGM : AA/Ag–Ni catalyst containing 0.9%Me. Its reuse leads to only a minor loss of the activity.

ACKNOWLEDGMENTS

The study was performed at the Research Institute of Chemical Problems, Buketov State University, Karaganda, Kazakhstan and on the base of the Chair of Analytical and Inorganic Chemistry, Charles University, Prague, Czech Republic.

REFERENCES

1. Sergeev, V.G., *Nanokhimiya* (Nanochemistry), Moscow: Mosk. Gos. Univ., 2003.
2. Olenin, A.Yu. and Lisichkin, G.V., *Russ. Chem. Rev.*, 2011, vol. 80, no. 3, pp. 605–630.
3. Xu, R., Xie, T., Zhao, Y., and Li, Y., *Cryst. Growth Des.*, 2007, vol. 7, no. 9, pp.1904–1911.
4. Suzdalev, I.P., *Nanotekhnologiya: fiziko-khimiya nanoklasterov, nanostruktur i nanomaterialov* (Nanotechnology: Physical Chemistry of Nanoclusters, Nanostructures, and Nanomaterials), Moscow: KomKniga, 2006.
5. Egorova, E.M., Revina, A.A., Rostovshchikova, T.N., and Kiseleva, O.I., *Vestn. Mosk. Univ., Ser. Khim.*, 2001, vol. 42, pp. 332–338.
6. Bekturov, E.A., Iskakov, R.M., and Shmakov, C.Y., *Sci. Central Asia*, 2010, no. 23, pp. 34–37.
7. Liu, X.W., *Langmuir*, 2011, vol. 27, no. 15, pp. 9100–9104.
8. Baranov, D.A. and Gubin, S.P., *Nanosistemy*, 2009, vol. 1, no. 1, pp. 129–147.
9. Burkeev, M.Zh., Khamitova, T.O., Havliček, D., Tazhbaev, E.M., Davrenbekov, S.Zh., and Kozhabekova, G.E., *Katal. Prom–sti.*, 2018, vol. 18, no. 3, pp. 6–13.
10. Kirilyus, I.V., *Elektrokataliticheskoe gidrirovanie* (Electrocatalytic Hydrogenation), Alma-Ata: Nauka Kaz. SSR, 1981.
11. Pomogailo, A.D. and Kestelman, V.N., *Metallopolymer nanocomposites*, Heidelberg: Springer, 2005.
12. Pomogailo, A.D., *Kinet. Catal.*, 2004, vol. 45, no. 1, pp. 61–103.